

Outlying H α emitters in SDSS IV MaNGA

Omkar Bait,^{1*}, Yogesh Wadadekar^{1†}, Sudhanshu Barway,^{2‡}

¹*National Centre for Radio Astrophysics, Tata Institute of Fundamental Research, Post Bag 3, Ganeshkhind, Pune 411007, India*

²*Indian Institute of Astrophysics (IIA), II Block, Koramangala, Bengaluru 560 034, India*

Accepted XXX. Received YYY; in original form ZZZ

ABSTRACT

We have carried out a systematic search for outlying H α emitters in the entire data release 14 of the Sloan Digital Sky Survey (SDSS) IV Mapping Nearby Galaxies at APO (MaNGA) survey. We have discovered six outlying H α emitters with no bright underlying optical continuum emission in the imaging data release 5 from the Dark Energy Camera Legacy Survey (DECaLS) and data release 6 of the Mayall z-band Legacy Survey (MzLS) + Beijing-Arizona Sky Survey (BASS). They also show a velocity field which is different from that of the host galaxy. These outlying H α emitters all have extended structure in the H α image. Their emission line ratios show that they are photoionised due to an active galactic nucleus (AGN) or a mixture of both an AGN and star formation. Some of them are very likely to be fainter counterparts of Hanny’s Voorwerp like objects.

Key words: galaxies: active — galaxies: star formation — galaxies: statistics — galaxies: evolution — galaxies: general

1 INTRODUCTION

Large-scale galactic outflows due to both starbursts and active galactic nuclei (AGN) are quite common, particularly at high redshifts, and play an important role in providing feedback in galaxy formation and evolution (see [Veilleux et al. 2005](#), for a review). Such galaxy outflows can appear as H α emission away from the galaxy. The classic example is that of Messier 82 (M82) which shows large scale bipolar superwinds ([Bland & Tully 1988](#); [Shopbell & Bland-Hawthorn 1998](#)) due to the ongoing starburst at the centre. Interestingly, M82 also shows an H α cap like structure at a projected distance of about 11 kpc from the disc ([Devine & Bally 1999](#); [Lehnert et al. 1999](#)). Typically such galactic outflows are known to trigger star formation in the host galaxy as a consequence of gas compression. However, [Maiolino et al. \(2017\)](#) has also found observational evidence for star formation occurring in the galactic outflow at a rate of more than 15 solar masses per year.

Another interesting case of an outlying emission line region is that of the Hanny’s Voorwerp ([Lintott et al. 2009](#)), discovered serendipitously, lying near the spiral galaxy IC 2497. This object was discovered as part of the Galaxy Zoo project in the Sloan Digital Sky Survey (SDSS) g-band image due to its strong emission in the [OIII]4959, 5007 lines.

It has been suggested that the gas in Hanny’s Voorwerp has a tidal origin ([Józsa et al. 2009](#)). This gas was then photoionised by the nucleus of IC 2497, which, in turn, was a quasi-stellar object (QSO) that has faded dramatically in the last 10⁵ years, thus producing a quasar light echo ([Lintott et al. 2009](#); [Schawinski et al. 2010](#)). In [Keel et al. \(2012b\)](#), Galaxy Zoo volunteers have carried out further searches to identify 19 more such objects, which are termed as extended emission-line regions (EELRs). Of these, most are in interacting or merging state which further makes the tidal origin of gas which was photoionised by an AGN a more plausible explanation of EELRs.

With the advent of large scale integral field unit (IFU) surveys e.g., the Mapping Nearby Galaxies at Apache Point Observatory ([Bundy et al. 2015](#), MaNGA), Calar Alto Legacy Integral Field Area survey ([Sánchez et al. 2012](#), CALIFA), and the Sydney-AAO Multi-object Integral-field spectrograph Galaxy survey ([Bryant et al. 2015](#), SAMI) we can now search for such outlying H α emitters around several thousand galaxies. In the MaNGA survey, [Cheung et al. \(2016\)](#) found an outlying H α complex without any optical counterpart about 6.3 kpc away from the effective radius of the host galaxy and at about 3 times the effective radius of the galaxy. Using a detailed analysis of the gas kinematics, gas phase metallicity, and emission-line ratios the authors argue that the scenario is most consistent with an gas accretion event. Recently, [Lin et al. \(2017\)](#) have discovered a large outlying H α blob (~ 3 -4 kpc in radius) around 8 kpc away from the host galaxy which is undergoing a dry galaxy

* E-mail: omkar@ncra.tifr.res.in (OB)

† E-mail: yogesh@ncra.tifr.res.in (YW)

‡ E-mail: sudhanshu.barway@iia.res.in (SB)

merger. Here the authors argue that this could either be an AGN outburst or a possible “ultra-diffuse galaxy”. Using the SAMI survey, [Fogarty et al. \(2012\)](#) have discovered an outlying emission-line region off the plane of the disk of edge-on galaxy ESO 185-G031 which is ionised due to shock excitation from a starburst driven wind. [Richards et al. \(2014\)](#) have found a large H II complex in the dwarf galaxy GAMA J141103.98–003242.3 which is similar to the Large Magellanic Cloud (LMC) and 30 Doradus complex. Recently, using the Multi Unit Spectroscopic Explorer (MUSE), [Epinat et al. \(2018\)](#) has found a large diffuse ionised gas complex ($\sim 10^4$ kpc² in area) in [OII] $\lambda\lambda 3727, 3729$ in a galaxy group COSMOS-Gr30 at a redshift of 0.725 with two kinematic sub-structures. The authors argue that atleast one of the gas component has a non-primordial origin arising either due to tidal interactions between the group galaxies or gas expelled due to AGN outflows. More recently, [Lopez Cobra et al. \(2018\)](#) have conducted a systematic search for galaxy outflows in the Local Universe using the CALIFA survey and have found 17 objects which show evidence of galactic winds. They find that these objects do not show any excess in the their integrated star formation rates (SFRs) compared to normal star forming galaxies. However, the SFR density in the inner regions shows an excess and is an important driver of galaxy outflows.

Thus a systematic study of outlying H α emitters is important from the point of view of understanding galaxy outflows and interestingly also in-situ star formation in these extreme environments. With a view to increase the sample size of these interesting but rare class of objects, we have carried a systematic search of outlying H α emitters in the recently released SDSS IV MaNGA IFU survey. We use the recently released MaNGA value added catalogue, analysed using the Pipe3D pipeline ([Sánchez et al. 2016b, 2018](#)), of 2,755 galaxies (see Sec. 2 for details on the sample selection). We visually identify outlying H α emitting regions around MaNGA target galaxies on which the IFU is centered. These emission line regions also shows a different velocity component from that of the host galaxy. Note that our search criteria differ from those of [Lopez Cobra et al. \(2018\)](#), where they have used various diagnostic diagrams (e.g., EW(H α), [NII]/H α line ratios etc.) which are tuned to find galactic winds, whereas we are interested in finding extended emission line regions away from the MaNGA target galaxies. We have found a total of six such outlying H α emitters which have extended H α structure around the host galaxies (see Sec. 2). Interestingly using the Baldwin Philip and Terlevich (BPT) diagram, we find that the extended H α emitters shows various sources of ionisation (see Section 3.1.1). In section 3.2 we briefly discuss the possibility that these extended emitters are low luminosity counterparts of Hanny’s Voorwerp ([Lintott et al. 2009](#)) like objects. In section 4 we briefly discuss some of the interesting sources in our sample. We will then summarise and conclude in Sec 5.

Throughout this paper we use the standard concordance cosmology with $\Omega_M = 0.3$, $\Omega_\Lambda = 0.7$ and $h_{100} = 0.7$.

2 SAMPLE SELECTION

Our sample is drawn from Mapping Nearby Galaxies at Apache Point Observatory ([Bundy et al. 2015](#), MaNGA)

survey which was released as part of the Sloan Digital Sky Survey Data Release 14 ([Abolfathi et al. 2017](#), SDSS DR14). This recent data release contains a sample of 2,812 MaNGA datacubes. These datacubes were analysed using the Pipe3D data analysis pipeline by the MaNGA team and their final catalogue of 2,755 galaxies forms our sample, wherein we search for outlying H α emitters.

2.1 The MaNGA survey

MaNGA is an integral field unit (IFU) survey which aims to observe a total sample of $\sim 10,000$ nearby galaxies. The MaNGA instrument consists of 17 hexagonal shaped science IFUs mounted on the 2.5 metre Apache Point Observatory which has a 3° field of view. The IFU sizes range from 19 fibres with $12''$ on-sky diameter to 127 fibres with $32''$ on-sky diameter. Additionally, there are 12 mini-bundles with 7 fibres each which are used for spectrophotometric calibration, and 92 single fibres used for sky subtraction. The details of the MaNGA instrument are described in [Drory et al. \(2015\)](#). The MaNGA fibres are then fed to the two Baryon Oscillation Sky Survey (BOSS) spectrographs ([Smee et al. 2013](#)), each of which contain a red and a blue camera which together have a wavelength coverage from 3600 Å to 10300 Å and a spectral resolution, $R \sim 2000$. The integration time for each of the MaNGA targets depends on the signal to noise ratio requirement of $5 \text{ Å}^{-1} \text{ fibre}^{-1}$ in r -band continuum at a surface brightness of $23 \text{ AB arcsec}^{-2}$ ([Law et al. 2015](#)). The raw data are then reduced using the MaNGA Data Reduction Pipeline (DRP) as described in [Law et al. \(2016\)](#), which constructs the sky subtracted and flux calibrated datacubes for each of the MaNGA galaxies. The MaNGA PSF can be well described by a single Gaussian with median spatial resolution of $\sim 2.54 \text{ arcsec FWHM}$. The median instrumental velocity resolution is 72 kms^{-1} . The typical relative flux calibration errors are 1.7% between H α and H β , and about 4.7% between [N II] $\lambda 6583$ and [O II] $\lambda 3727$ ([Yan et al. 2016](#)).

The primary MaNGA selection criteria produce a sample of roughly 10,000 galaxies which is complete above the stellar mass limit of $10^9 M_\odot$ and has a roughly flat stellar mass distribution (See [Bundy et al. 2015](#); [Wake et al. 2017](#)). More constraints are put in order to maximise spatial coverage and S/N which favours a lower redshift sample. Other constraints favour a higher redshift sample. Taking these constraints into account the MaNGA target galaxies are divided into two classes: Primary and Secondary samples. The Primary sample has a mean redshift of 0.03 and reaches 1.5 times the galaxy half-light radius (R_e) for roughly 80% of its targets. The Secondary sample has a slightly higher mean redshift of 0.045 and reaches $2.5 R_e$ for roughly 80% of its targets. Of the total target sample of $\sim 10,000$ galaxies, the data release 14 contains a sample of 2,812 reduced MaNGA datacubes.

2.2 PIPE3D value added catalogue

In this study, we use the MaNGA value added catalogue analysed using the PIPE3D pipeline ([Sánchez et al. 2016b, 2018](#)) which is based on FIT3D, the details of which are described in [Sánchez et al. \(2016a\)](#). We briefly describe the fitting algorithm here.

FIT3D follows a two level modelling of the integral field spectroscopy (IFS) data. At the first level, it models the stellar kinematics, stellar population and dust attenuation using the continuum. At this level, initially the stellar kinematics (only the velocity and dispersion) are estimated assuming a Gaussian profile¹. This is achieved by first fixing the velocity dispersion and varying the velocity from the minimum to the maximum value until a best fit velocity is found. Then the velocity is fixed to the best fit value and the velocity dispersion is varied till the best-fit value is found. Following this, the dust attenuation is varied until the best fit dust attenuation is found, while keeping the velocity and velocity dispersion fixed to their best fit values. Once the best fit value of these three parameters are found FIT3D performs the stellar population synthesis (SPS) modelling using the GSD16 stellar template library (Cid Fernandes et al. 2013). GSD16 contains a total of 156 templates with 39 stellar ages, ranging from 1 Myr to 13 Gyr, and 4 metallicities: 0.2, 0.4, 1, and 1.5 times solar metallicity. Each of these templates are shifted according to the velocity, convolved with the velocity dispersion and dust attenuated, following the dust attenuation law of Cardelli et al. (1989), using the best fit values of the individual parameters. The average properties of the stellar population (e.g., stellar mass, light/mass weighted stellar age, metallicity, mass-to-light ratio, etc.) is derived using the weights on the individual single stellar population.

The second level of FIT3D deals with the measurement of nebular emission lines. The emission line only spectrum is derived by subtracting the modeled stellar continuum obtained from the previous level. The uncertainties involved in the stellar population modelling are propagated to the emission line-only spectrum. Thereafter, around each emission line a single Gaussian and a low order polynomial is fitted. Following a similar procedure as in the previous level, the velocity, velocity dispersion and the intensity of each line is derived starting by first fitting for the velocity and fixing the other two parameters. This is followed by fitting for the velocity dispersion and finally for the intensity of the emission line. Furthermore, the $H\alpha$ emission line is corrected for dust attenuation using the Balmer decrement for every spaxel assuming a $H\alpha/H\beta$ line ratio of 2.86 and adopting a Cardelli et al. (1989) dust attenuation law and specific dust attenuation of R_V of 3.1.

The current data release of the PIPE3D value added catalogue² has provided dataproducts and catalogue for 2,755 galaxies in the MaNGA sample.

2.3 Optical Photometric data

We also use the publicly available optical g , r , and z band imaging data from the SDSS DR14, which have a 5σ depths of 23.13, 22.7 and 20.71 respectively. We also use the data release 5 of the Dark Energy Camera Legacy Survey (DECaLS) and data release 6 of the Mayall z -band Legacy Survey (MzLS) + Beijing-Arizona Sky Survey (BASS). The DECaLS survey is being carried out on the Dark Energy

Camera (DECam) on the Blanco 4m telescope at the Cerro Tololo Inter-American Observatory and it will provide the optical imaging for the Dark Energy Spectroscopic Instrument (DESI) footprint. DECam with its large field of view and good sensitivity can reach a 5σ depths of 24.0, 23.4 and 22.5 in the g , r , and z band respectively. The BASS survey is being carried out on the 2.3m Bok telescope using the 90Prime camera in the g and r band, and it will reach similar 5σ depths of 24.0 and 23.4 in g and r band respectively. Similarly the MzLS survey is being carried out on the Mayall telescope at Kitt Peak National Observatory using the MOSAIC-3 camera only in the z -band and will reach a 5σ depth of 23.0.

2.4 Selection Criteria

We identify a region of $H\alpha$ emission as an outlying $H\alpha$ emitter if the following three criteria are satisfied:

- (i) A signal-to-noise ratio (SNR) of $H\alpha$ flux greater than 5 and which covers atleast one MaNGA PSF which corresponds to ~ 5 spaxels.
- (ii) No bright optical counterpart in SDSS gri colour composite image or in the DECaLS, MzLS/BASS gri colour composite image.
- (iii) $H\alpha$ velocity of the emitter which is different (typically upto 400 km/s) from the velocity field of the parent galaxy and/or the $H\alpha$ emission is clearly extra-planar.

Under these criteria, we follow a fairly straightforward, two step approach, to visually search for such outlying $H\alpha$ emitters. In the first step we select galaxies which satisfy the first two criteria. To do this, we produce panels for each galaxy in the MaNGA sample having the DECaLS/MzLS-BASS colour image and the $H\alpha$ flux map. We visually inspect each galaxy using this panel and search for $H\alpha$ emitting regions which do not show any bright optical counterpart. Starting from a sample of 2,755 MaNGA galaxies released in the PIPE3D catalogue, we visually identify 133 galaxies which satisfy these two criteria.

In the second step, we inspect the $H\alpha$ velocity map of these shortlisted galaxies to make sure that the outlying $H\alpha$ emission is different from that of the host galaxy. Fig. 1, shows an example of an outlying $H\alpha$ emitter in our sample. Notice the large scale $H\alpha$ emission away from the optical extent (first and second panel) of the host galaxy highlighted in red ellipses. The $H\alpha$ velocity of the outlying emission is also different from that of the optical galaxy shown as seen from the third and fourth panels. Such a galaxy satisfies all the three selection criteria and is added in the sample of outlying $H\alpha$ emitting region. We visually inspect the velocity map of all the 133 shortlisted galaxies in the first step of the selection and find a final sample of 41 galaxies which satisfy all the three selection criteria.

We then individually inspect the spectrum of these outlying $H\alpha$ emitters and find that 35 objects are artefacts since the FWHM of the $H\alpha$ line is very narrow ($\sim 2 \text{ \AA}$) compared to the instrumental width of the MaNGA IFU. Of them about 29 of them appear like hot-pixels in the $H\alpha$ image as shown in Fig. 2, and 6 have extended emission but a very narrow $H\alpha$ FWHM. Notice that Fig. 2, shows the outlying emission with a very high SNR (as shown in red circle) and also has a

¹ FIT3D does not model higher order kinematics as it is primarily developed for lower spectral resolution ($R < 2000$) IFS.

² <http://www.sdss.org/dr14/manga/manga-data/manga-pipe3d-value-added-catalog/>

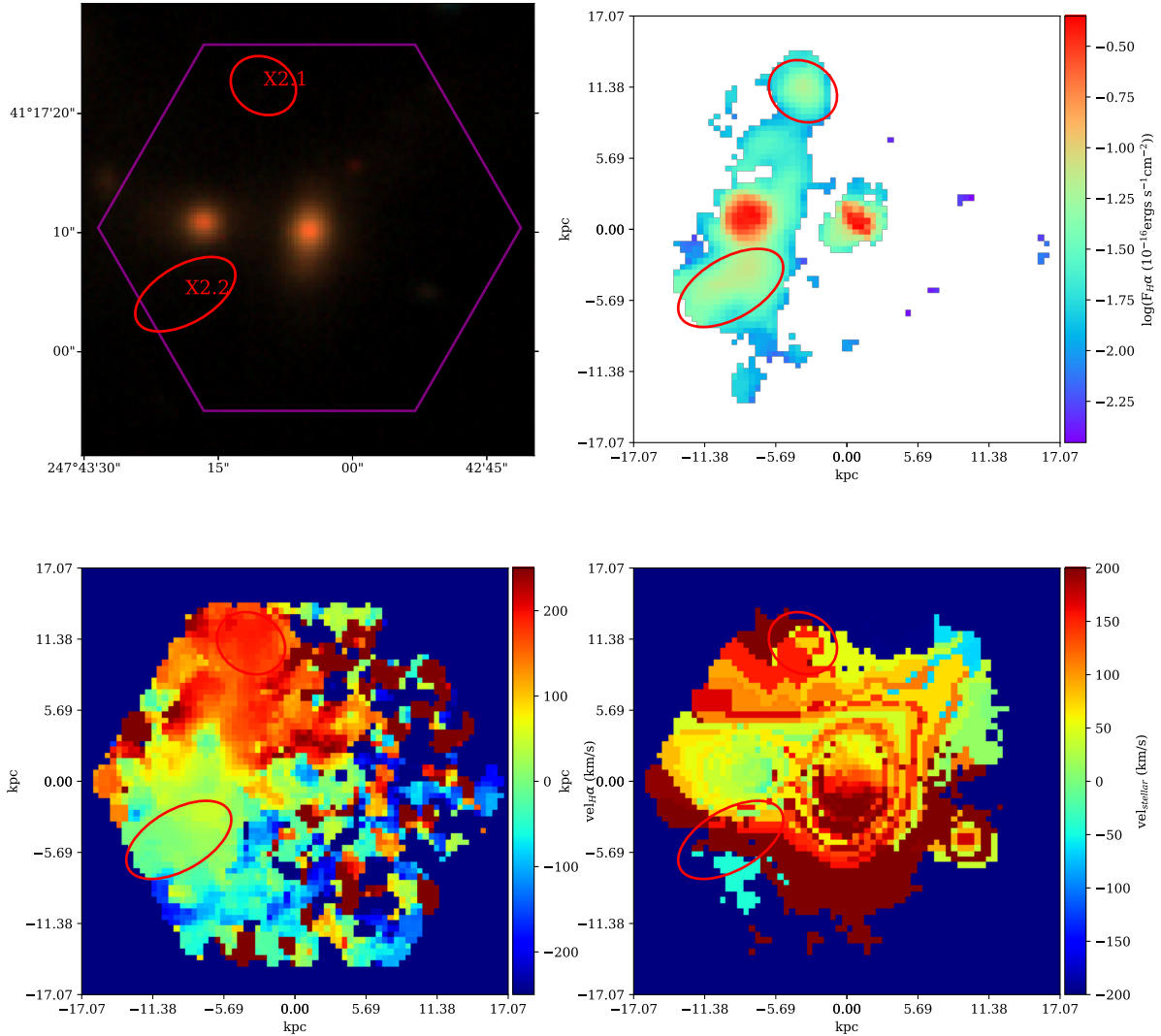


Figure 1. MaNGA observation of a galaxy with MaNGA ID: manga-8601-12701. Top-left: MzLS/BASS grz Lupton et al. (2004) colour composite image with the MaNGA IFU extent around the galaxy shown in purple in world coordinate system (WCS). Top-right: $H\alpha$ flux map in logarithmic units. Bottom-left: $H\alpha$ velocity map. Bottom-right: Stellar velocity map of the host galaxy. The outlying $H\alpha$ emitters are circled in red in all the panels. Notice that the $H\alpha$ emitter does not have any bright optical counterpart, it also has a velocity component different from the host galaxy.

very different velocity component from the host galaxy, however after visually inspecting the spectrum it is flagged as an artefact. The full list of artefacts in the MaNGA survey is given in the Appendix B, which is available in the online version of this paper. Our final sample of outlying $H\alpha$ emitters is summarised in Table 1. We have also independently rediscovered the outlying $H\alpha$ emitter from Lin et al. (2017), but do not discuss it here as it has been extensively studied in their paper.

3 RESULTS AND DISCUSSIONS

In this section, we measure the integrated emission line fluxes using aperture photometry of the outlying $H\alpha$ emitters. We then study their position on the emission line ratio diagnostic diagram of Baldwin et al. (1981). Finally, we individually describe the objects in our sample.

3.1 Integrated properties of outlying $H\alpha$ emitters

In this section, we study the integrated emission line fluxes of the outlying $H\alpha$ emitters from our sample. In particular, in order to know the source of ionisation we want to identify the location of these outlying $H\alpha$ emitters on the “BPT diagram” (Baldwin et al. 1981). Hence, we measure the total emission line flux in the $H\alpha$, $[\text{NII}]\lambda 6583$, $[\text{OIII}]\lambda 5007$, and the $\text{H}\beta$ lines.

We make elliptical apertures³ around all the extended $H\alpha$ emitters (xHAEs) to estimate the total $H\alpha$ flux. We similarly construct the $[\text{NII}]$, $[\text{OIII}]$, $[\text{SII}]\lambda 6717$, 6731 and $\text{H}\beta$ emission line maps, and measure the total flux in each of the emission lines respectively. We also estimate the total error in the emission line flux inside the aperture by adding

³ The aperture photometry was performed using the photutils package <https://photutils.readthedocs.io/en/stable/>.

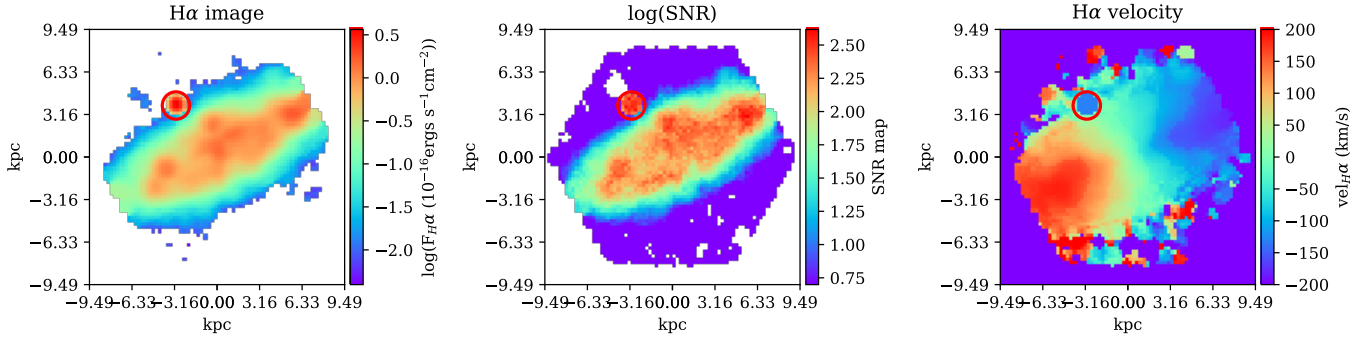


Figure 2. MaNGA observation of a spiral galaxy with MaNGA ID: manga-8257-12703. Left panel: $H\alpha$ flux map in logarithmic units. Middle panel: $H\alpha$ logarithm of the signal to noise ratio with truncation below SNR of 5. Note that the apparent outlying $H\alpha$ emitter which satisfies all the criteria and circled red is an artefact since it has a very narrow emission line width as seen in the MaNGA datacube (not shown here). The full list of such artefacts is given in the Appendix B.

Table 1. Final Sample of outlying $H\alpha$ emitters in the SDSS MaNGA.

Obj ID	RA J2000 (hhmmss)	DEC J2000 (ddmmss)	plate-ifu	Host SDSS Obj ID	RA (Host) J2000 (deg)	DEC (Host) J2000 (deg)	z
X1	14:09:06.710	+53:27:55.644	8591-6101	1237661416601878596 (HX1)	14:09:06.87	+53:27:48.70	0.0785
X2.1	16:30:52.685	+41:17:22.074	8601-12701	1237655374109802661 (HX2)	16:30:53.11	+41:17:10.81	0.0936
X2.2	16:30:53.268	+41:17:04.565	8601-12701	1237655374109802661 (HX2)	16:30:53.11	+41:17:10.81	0.0936
X3	08:47:47.430	+54:01:29.807	8724-6102	1237651533336281291 (HX3)	08:47:46.76	+54:01:36.02	0.0472
X4	08:18:50.238	+22:57:14.864	8939-12701	1237661085345513774 (HX4)	08:18:49.61	+22:57:16.37	0.0924
X5	11:15:47.004	+50:24:09.997	8947-3701	1237657855533056062 (HX5)	11:15:47.46	+50:24:05.75	0.0475

Notes. Column (1) gives the object ID of the outlying $H\alpha$ emitter, column (2) and (3) gives the RA and DEC of the outlying $H\alpha$ emitter respectively. Column (4) and (5) gives the MaNGA plateifu name and SDSS DR14 object ID of the host galaxy respectively. And columns (6), (7) and (8) give the RA and DEC and SDSS spectroscopic redshift of the host galaxy respectively.

the error in each spaxel in quadrature. We do this for each of the four emission line maps and for all the outlying $H\alpha$ emitters in our sample. Table 2 shows the integrated fluxes of the individual sources in our sample. We also extracted the integrated spectrum in these apertures for each source from the MaNGA datacube which is shown in Appendix A available with the online version of this paper.

3.1.1 BPT diagram

In this section, we use the BPT diagnostic diagram to identify the source of ionisation in the outlying $H\alpha$ emitters. The BPT diagram is widely used to classify galaxies into star forming (SF), Seyferts, and low-ionisation emission line regions (LINERs) (e.g., Kewley et al. 2006; Kauffmann et al. 2003). The BPT classification scheme is also used in resolved IFU studies (e.g., Belfiore et al. 2016; Lin et al. 2017). In our study we use the $[OIII]\lambda 5007/H\beta$ vs. $[NII]\lambda 6583$ ($[SII]\lambda 6717, 6731/H\alpha$) diagram. For simplicity, we will refer to the $[OIII]\lambda 5007$, $[NII]\lambda 6583$, $[SII]\lambda 6717, 6731$ (which is the sum of the two lines) as $[OIII]$, $[NII]$, and $[SII]$ respectively.

Figure 3 left (right) panel shows the $[OIII]/H\beta$ vs.

$[NII]/([SII])/H\alpha$ diagnostic diagram for our sample of outlying $H\alpha$ emitters. The corresponding line ratios for the host galaxies are determined using SDSS DR14 spectroscopy. In both the panels the red solid line is for the theoretical maximum starburst line from Kewley et al. (2006) which we refer as the Ke06 line hereafter. And the black dashed line in the left panel is semi-empirical line from Kauffmann et al. (2003) which we refer to as the Ka03 line hereafter. In the $[NII]/H\beta$ BPT diagram the source of ionisation for the region below the Ka03 line is purely from star formation. For the region above the Ke01 line the source of ionisation is from a type 2 AGN wherein it is from a Seyfert AGN if it is above the blue solid line and LINER if it is below the blue solid line (Cid Fernandes et al. 2010). For the region between the Ka03 and Ke01 lines the source of ionisation is from a mix of star formation and non-star formation, and it is termed as “composite”. Moreover, ionisation due to slow shocks has been also shown to push the points into the LINER region (Farage et al. 2010; Rich et al. 2010). In the $[SII]/H\alpha$ BPT diagram, the region below the Ke06 line has ionisation purely due to star formation. The region above the Ke06 line and above the blue line has ionisation due to Seyfert AGN and region

Table 2. Integrated fluxes and uncertainty of $H\alpha$, [OIII], [NII], $H\beta$, [SII] λ 6717, and [SII] λ 6731 emission lines for the extended outlying $H\alpha$ emitters.

Obj ID	$F_{H\alpha}$ ($\sigma_{H\alpha}$)	$F_{[OIII]}$ ($\sigma_{[OIII]}$)	$F_{[NII]}$ ($\sigma_{[NII]}$)	$F_{H\beta}$ ($\sigma_{H\beta}$)	$F_{[SII]\lambda 6717}$ ($\sigma_{[SII]\lambda 6717}$)	$F_{[SII]\lambda 6731}$ ($\sigma_{[SII]\lambda 6731}$)	BPT classification
X1	2.166 (0.033)	0.884 (0.053)	0.894 (0.038)	0.595 (0.048)	2.004 (0.117)	0.302 (0.113)	composite/LINER
X2.1	2.641 (0.033)	1.39 (0.044)	0.804 (0.042)	0.772 (0.037)	0.472 (0.065)	0.256 (0.072)	composite/star forming
X2.2	7.323 (0.039)	15.332 (0.098)	2.208 (0.067)	2.357 (0.053)	1.338 (0.102)	0.549 (0.092)	Seyfert
X3	2.464 (0.037)	0.778 (0.055)	0.565 (0.05)	0.594 (0.064)	1.027 (0.034)	0.368 (0.04)	star forming
X4	4.085 (0.051)	9.535 (0.102)	5.525 (0.12)	1.603 (0.091)	3.655 (0.16)	1.672 (0.17)	Seyfert/LINER
X5	4.218 (0.055)	7.1 (0.087)	0.45 (0.065)	1.421 (0.066)	0.525 (0.056)	0.403 (0.052)	star forming/Seyfert

Notes . Column (1) gives the object ID of the outlying $H\alpha$ emitter. Columns (2), (3), (4), (5), (6) and (7) give the total flux and 1σ uncertainty for the $H\alpha$, [OIII], [NII], $H\beta$, [SII] λ 6717 and [SII] λ 6731 line respectively. For non-detections, the fluxes are replaced by the 3σ upper limits. All values are in units of $10^{-16} \text{ ergs s}^{-1} \text{ cm}^{-2}$. Column (8) gives the BPT classification of the xHAEs. See Sec. 3.1.1 for details.

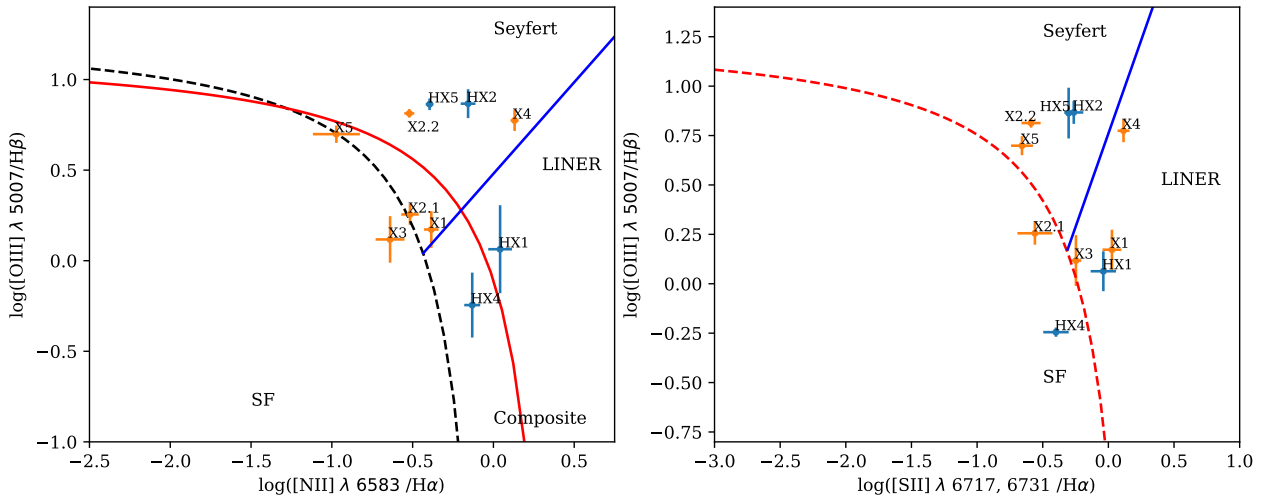


Figure 3. Left Panel: The [OIII]/ $H\beta$ vs. [NII]/ $H\alpha$ BPT diagnostic diagram. The red solid line is the extreme starburst line from Kewley et al. (2006, Ke06). The black dashed line is from the semi-empirical fit to the SDSS galaxies from Kauffmann et al. (2003, Ka03). The region below the Ka03 line is termed as star-forming (SF) region. In the region above the Ke06 and Ka03 line is termed as composite region, which has emission from both star formation and AGN. Right Panel: The [OIII]/ $H\beta$ vs. [SII] λ 6717, 6731/ $H\alpha$ BPT diagnostic diagram. The red dashed line is the extreme starburst line from Kewley et al. (2006, Ke06). The extended $H\alpha$ emitters are shown in orange dots. These show various sources of ionisation in their spectrum. The blue points are for the corresponding host galaxy. See the text for details.

above the Ke06 line and below the blue line has ionisation due to LINER like AGN.

In Figure 3, the most striking result is that of X2.2, which is classified as ionized due to a Seyfert AGN in both the diagrams. X2.1, which is at the edge of extreme starburst line in the [NII]/ $H\alpha$ BPT diagram, has moved within the starburst line in the [SII]/ $H\alpha$ diagram. Interestingly, the corresponding host galaxy (HX2) has a Seyfert AGN in the centre, which provides the ionising photons for X2.2, thus putting it in the Seyfert region. X1 is classified as composite and LINER in the [NII]/ $H\alpha$ and the [SII]/ $H\alpha$ BPT diagrams respectively. The host (HX1) also shows a corresponding LINER emission line ratio in its centre. X4 is classified as Seyfert and LINER in the [NII]/ $H\alpha$ and the [SII]/ $H\alpha$ BPT diagram respectively. However, peculiarly the host (HX4) does not show any nuclear activity. X5 which is classified as at the edge of extreme starburst in the [NII]/ $H\alpha$ diagram is

shifted to the Seyfert region in the [SII]/ $H\alpha$ diagram. The host galaxy (HX5) also shows a Seyfert-like line ratios in the centre, and thus could be the source of ionisation. X3 is still consistent with being at the edge of extreme starburst line from both the BPT diagrams. The host galaxy (HX3) is devoid of any emission lines and thus does not have any nuclear activity or SF in the centre (and hence it is not shown in Figure 3).

Thus the extended emitters show a mix sources of ionisation ranging from star formation to composite emission. In particular X2.2 and X4 show clear signatures of Seyfert/LINER like emission line ratios. Except in the case of X4, the corresponding host galaxies have a active nuclei which could be the source of ionisation of these regions. The extended morphology and Seyfert/LINER like emission line ratios lead us to think that these objects are extended emission line regions (EELRs) e.g. the Hanny's Voorwerp

(Lintott et al. 2009; Keel et al. 2012a) and similar EELRs searched by the Galaxy Zoo candidates (Keel et al. 2012b), and Unger et al. (1987) and Tadhunter & Tsvetanov (1989). We describe each of these objects in detail in the next section.

3.2 Comparison of H α luminosities of xHAEs with literature

Keel et al. (2012b), using the Galaxy Zoo candidates, have carried out a systematic search for extended emission line regions (EELRs) and have documented 19 objects. A detailed study of the sources of ionisation in their EELRs shows that they are photoionised due to an AGN. The objects reported in our sample also show similar morphological features as those in the Keel et al. (2012b) sample and are also primarily photoionised due to an AGN. However, unlike their sample, our sample objects do not show any bright optical counterparts in deep optical images. The median values of the H α luminosities of our xHAEs is 4.47×10^{39} ergs/s. This is about 4.5 times fainter than the median H α luminosity of the Keel et al. (2012b) sample (2×10^{40} ergs/s). Thus, using our selection method with MaNGA data we are able to detect fainter counterparts of Hanny's Voorwerp like objects.

In conclusion, we find that the xHAEs have ionisation due to various kinds of sources ranging from Seyfert AGN, star formation and also a mixture of both. Moreover, their H α luminosities show that they are fainter counterparts of the EELRs.

4 REMARKS ON INDIVIDUAL SOURCES

In this section we will briefly describe the xHAEs in our sample.

(i) X1 (host SDSS objID: 1237661416601878596): As shown in the H α image in Figure 4, there is an extended outlying H α emission (highlighted with a red ellipse and referred to as X1). The host galaxy, which has an elliptical morphology (Graham et al. 2018, G18 hereafter), does not show any features of interaction in its light profile both at the location of the H α emission and elsewhere. The H α velocity map of the galaxy on the contrary shows very disturbed features. There appears to be some kind of rotation along the northeast-southwest diagonal axis, with the gas in the northeast direction moving away from us and the gas along the southwest direction coming towards us. The outlying H α emission on the other hand has a different velocity from this, and is coming towards us with a velocity of about 100 km/s. Moreover, the stellar velocity shown in the last panel is completely misaligned from the velocity flow of the H α emission. Such an misalignment is a signature of recent gas rich merger. X1 has a composite/LINER emission line ratios from the BPT diagram (see Table 2), and the host galaxy is classified has LINER like emission line ratios in the centre. This could be an example of Hanny's Voorwerp like object. However, unlike Hanny's Voorwerp X1 has no detectable optical counterpart and hence this object is likely a fainter counterpart of the Voorwerp.

(ii) X2.1 & X2.2 (host SDSS objID: 1237655374109802660): In Fig. 1, both X2.1 and X2.2

have emission coming from a merging system of two galaxies (G18). Here we identify the host galaxy not with the galaxy on which the MaNGA IFU is centered (ObjID: 1237655374109802660), but rather with the galaxy adjacent to it (ObjID: 1237655374109802661), due to the continuity of the H α emission with it. X2.1 has a velocity very near the velocity of the host galaxy and could be a case of extraplanar gas. This merger is caught in the MaNGA IFU field of view. The IFU is centred around the galaxy 8601-12701. X2.1 is at the edge of composite/star forming region, and X2.2 has Seyfert emission line ratios. The host galaxy (HX2) also has Seyfert AGN in the centre. It is intriguing to see that both X2.1 and X2.2 emitting regions which are on opposite sides of the host galaxy show a connected bridge. Moreover, the velocity map shows a gradient as we go along the connecting bridge around the host galaxy. Both X2.1 and X2.2 are examples of fainter counterparts of Hanny's Voorwerp.

(iii) X3 (host SDSS objID: 1237651533336281291, see Figure 5): The host galaxy has an elliptical morphology (G18) with no clear indication of recent merger/integration in its light profile. The host galaxy of X3 is however, devoid of any emission lines and thus does not have an active nucleus. Interestingly, X3 is a large star forming region, however it has a velocity which is very different (about 400 km/s) from the disc as seen in the stellar velocity profile (due to poor H α SNR of the host galaxy the velocity map is not visible). It is possible that this galaxy may have undergone a recent merger with a galaxy which may have left a tidal tail or there has been a recent event of gas accretion as in the case of Cheung et al. (2016). Given that there is such a high velocity difference, it is also possible that the H α emission is not associated with HX3, and is rather associated with a neighbouring galaxy (SDSS ObjID: 1237651252560461948), which is about 570 km/s offset from it, which also has an active nucleus. Thus, a past interaction with HX3 may have left a tidal tail, which is being photoionised by the neighbouring galaxy.

(iv) X4 (host SDSS objID: 1237661085345513774, see Figure 6): The host galaxy is a spiral galaxy with a close companion nearby (G18) and has a LINER/composite emission line ratios. It is possibly interacting with another early type galaxy. X4 has Seyfert/LINER like emission line ratio. The H α gas and stellar rotation is in the same direction although there is an misalignment between the two. X4 is also an example of Hanny's Voorwerp like object.

(v) X5 (host SDSS objID: 1237657855533056062, see Figure 7): X5, like X2.1 and X2.2, also shows a continuity with the host galaxy. The host of X5 is an S0 galaxy (G18) which has a Seyfert AGN in the centre. Interestingly, X5 is at the edge of the star forming/Seyfert region. The H α velocity map shows that the gas has very different velocity from the host galaxy and is moving away from the galaxy with a velocity of at least 300 km/s, which is fairly large. However, given the continuity in the H α emission with the host galaxy we believe that it is associated with it. It is possible that this is a event of outflowing gas due to AGN feedback, and this gas is undergoing in-situ star formation. Maiolino et al. (2017) have recently observed such an event of in-situ star formation in galactic outflows at a redshift of 0.0448. Intriguingly, the H α velocity map shows a gradient, and thus there are likely multiple velocity components in the emission region.

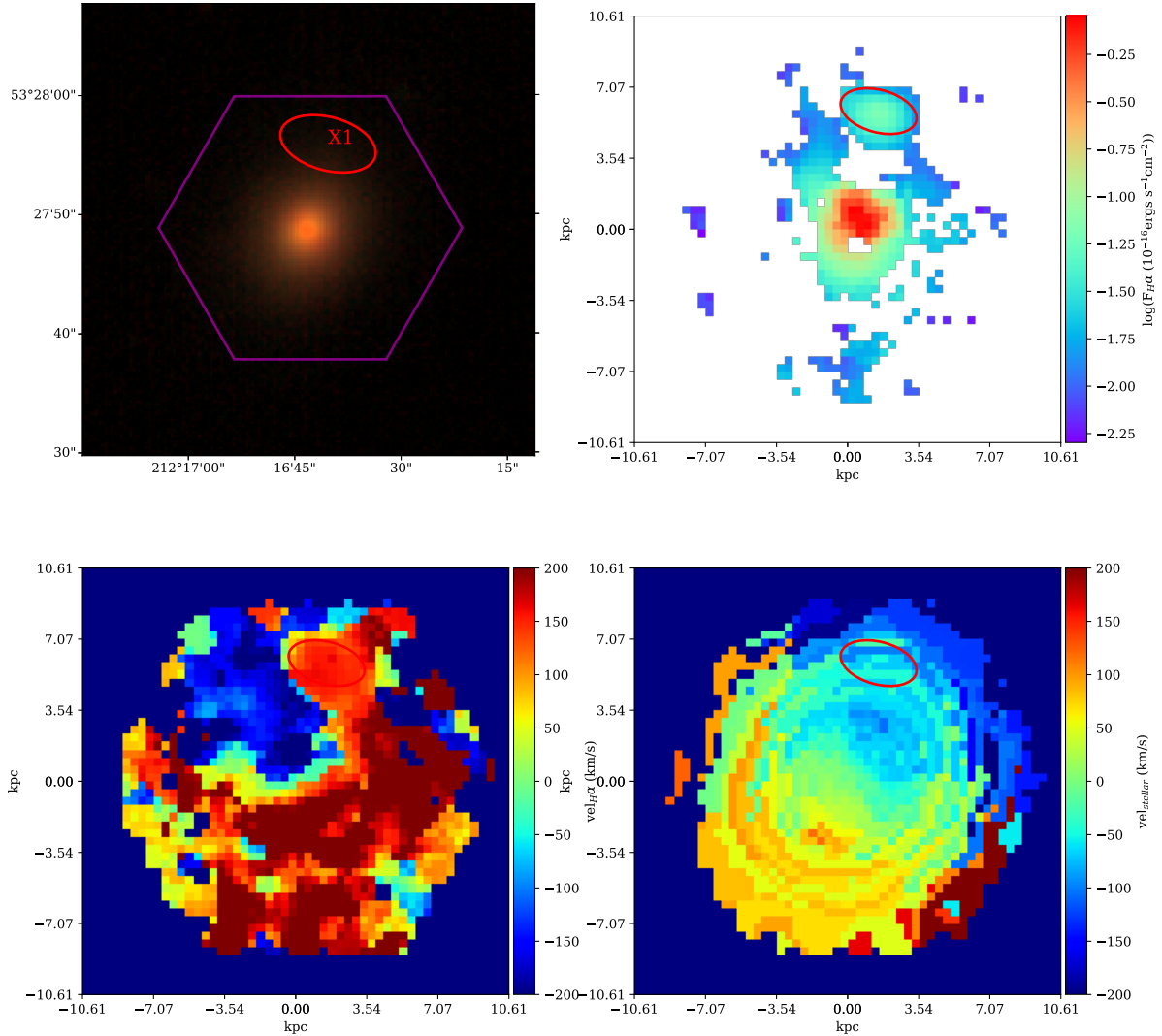


Figure 4. Top-left panel: Shows the DECals or MzLS-BASS *grz* Lupton et al. (2004) colour composite image of the host galaxies with the MaNGA IFU extent in purple. Top-right panel, bottom-left and bottom-right panel shows the $H\alpha$ emission map, $H\alpha$ velocity map and stellar velocity map respectively for X1 in physical units in kpc. In each panel the red ellipse highlights the location of the xHAEs. See text for details.

This feature is also seen in the integrated spectrum shown in the Appendix A (Figure A6), where we see two velocity components in the spectrum.

5 SUMMARY

In summary, we have conducted a systematic search for outlying $H\alpha$ emitters in the entire PIPE3D value added catalogue of the recently released DR14 SDSS IV MaNGA survey of 2,755 galaxies. We have found six outlying extended $H\alpha$ emitters (xHAEs) which have strong $H\alpha$ emission away from the host galaxy and without any bright optical continuum counterpart in the deeper optical images from the DECals or MzLS/BASS survey. These $H\alpha$ emitters also show a $H\alpha$ velocity component which is different from that of the host galaxy, ranging from about 150–400 km/s. We have also found several artefacts in the MaNGA datacubes most of which appear unresolved sources in the $H\alpha$ maps. However, their $H\alpha$ line-widths are much narrower than the

instrumental width of the MaNGA IFU. These are likely to be spurious cosmic rays which were not flagged by the MaNGA data reduction pipeline. The integrated line flux ratios show of the six xHAEs shows various kinds of sources of photoionisation. Three of the xHAEs show photoionisation due to an AGN, two of them have composite emission line ratio and one of them have photoionisation due to star formation. These xHAEs have $H\alpha$ luminosities at the lower end of the previously known EELRs and are thus their fainter counterparts.

Due to the poor spatial resolution of the MaNGA IFU it is very difficult to study the emission line regions with more detail, in particular since it can blend emission lines from two different, but spatially nearby, sources of ionisation into a single line. To address this limitation, we intend to follow-up these objects in our sample with a higher spatial resolution IFU e.g., SITELE (Spectromètre Imageur à Transformée de Fourier pour l’Etude en Long et en Large de raies d’Emission) on the Canada-France-Hawaii-Telescope

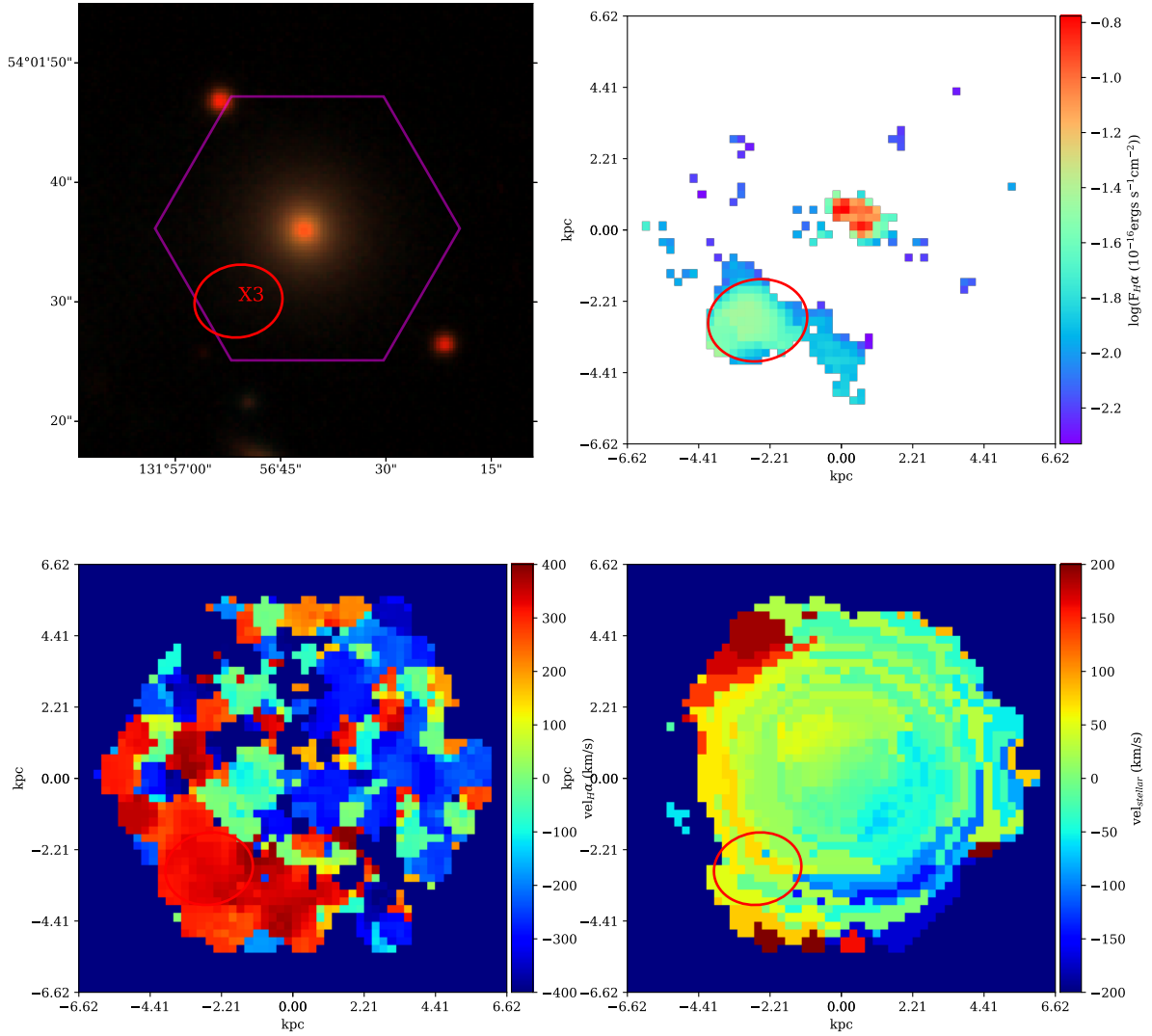


Figure 5. Continued. Here we show the outlying emission for X3.

(CFHT). This will also give us a larger field of view which can capture more emission line regions which are missed in the narrow field of view of MaNGA. Along with these new IFU observations, we also hope to obtain deep optical images to locate the optical counterparts of the H α emitters in our sample.

ACKNOWLEDGMENTS

We thank the anonymous referee for insightful comments that have improved both the content and presentation of this paper. We would also like to thank Alexei Moiseev for alerting us to artefacts in the MaNGA datacubes.

Funding for the Sloan Digital Sky Survey IV has been provided by the Alfred P. Sloan Foundation, the U.S. Department of Energy Office of Science, and the Participating Institutions. SDSS acknowledges support and resources from the Center for High-Performance Computing at the University of Utah. The SDSS web site is www.sdss.org.

SDSS is managed by the Astrophysical Research Consortium for the Participating Institutions of the SDSS Col-

laboration including the Brazilian Participation Group, the Carnegie Institution for Science, Carnegie Mellon University, the Chilean Participation Group, the French Participation Group, Harvard-Smithsonian Center for Astrophysics, Instituto de Astrofísica de Canarias, The Johns Hopkins University, Kavli Institute for the Physics and Mathematics of the Universe (IPMU) / University of Tokyo, Lawrence Berkeley National Laboratory, Leibniz Institut für Astrophysik Potsdam (AIP), Max-Planck-Institut für Astronomie (MPIA Heidelberg), Max-Planck-Institut für Astrophysik (MPA Garching), Max-Planck-Institut für Extraterrestrische Physik (MPE), National Astronomical Observatories of China, New Mexico State University, New York University, University of Notre Dame, Observatório Nacional / MCTI, The Ohio State University, Pennsylvania State University, Shanghai Astronomical Observatory, United Kingdom Participation Group, Universidad Nacional Autónoma de México, University of Arizona, University of Colorado Boulder, University of Oxford, University of Portsmouth, University of Utah, University of Virginia, University of Washington, University of Wisconsin, Vanderbilt University, and Yale University.

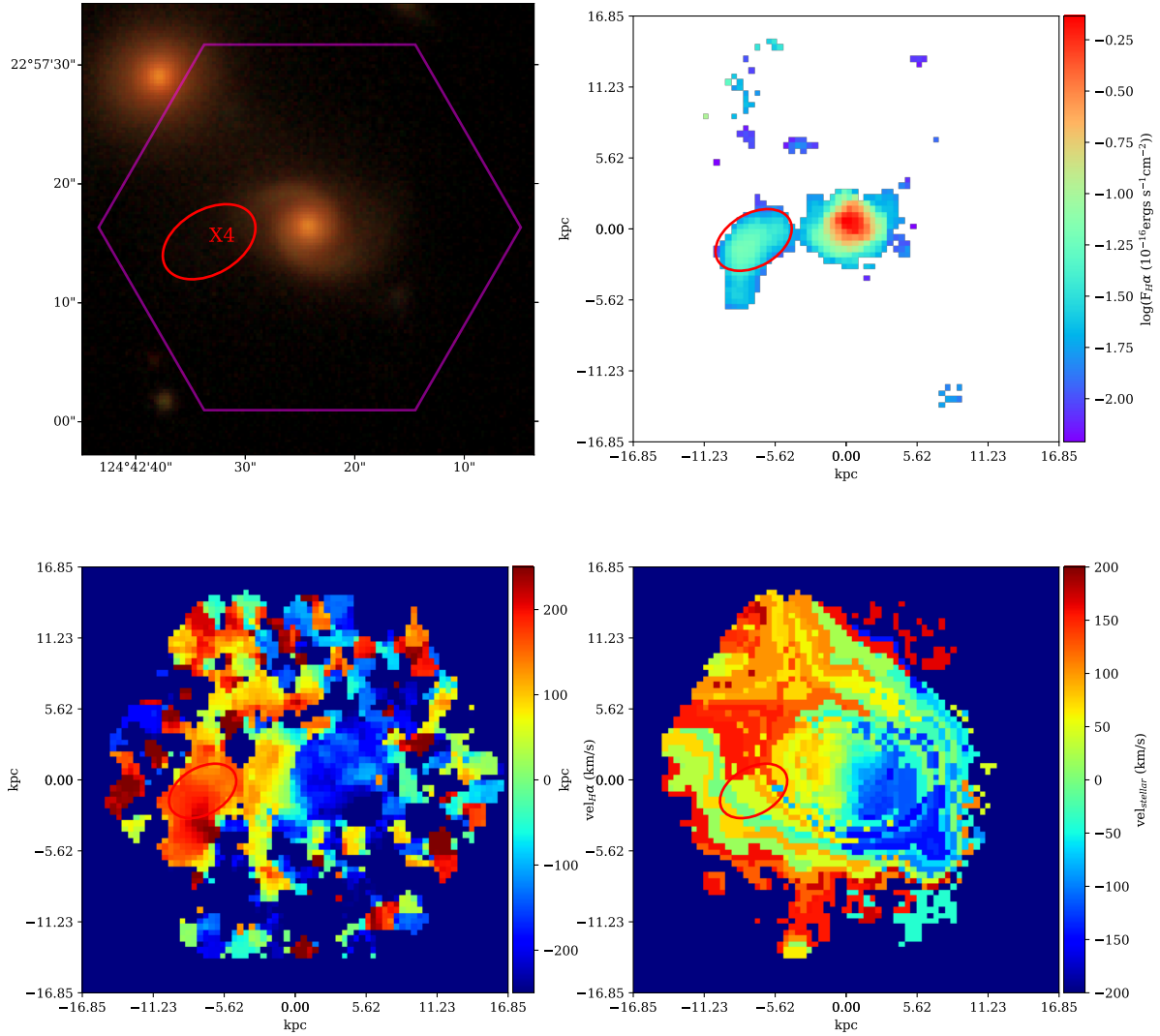


Figure 6. Continued. Here we show the outlying emission for X4.

This project makes use of the MaNGA-Pipe3D dataproducts. We thank the IA-UNAM MaNGA team for creating this catalogue, and the ConaCyt-180125 project for supporting them.

The Legacy Surveys consist of three individual and complementary projects: the Dark Energy Camera Legacy Survey (DECaLS; NOAO Proposal ID # 2014B-0404; PIs: David Schlegel and Arjun Dey), the Beijing-Arizona Sky Survey (BASS; NOAO Proposal ID # 2015A-0801; PIs: Zhou Xu and Xiaohui Fan), and the Mayall z-band Legacy Survey (MzLS; NOAO Proposal ID # 2016A-0453; PI: Arjun Dey). DECaLS, BASS and MzLS together include data obtained, respectively, at the Blanco telescope, Cerro Tololo Inter-American Observatory, National Optical Astronomy Observatory (NOAO); the Bok telescope, Steward Observatory, University of Arizona; and the Mayall telescope, Kitt Peak National Observatory, NOAO. The Legacy Surveys project is honored to be permitted to conduct astronomical research on Iolkam Du'ag (Kitt Peak), a mountain with particular significance to the Tohono O'odham Nation.

NOAO is operated by the Association of Universities for

Research in Astronomy (AURA) under a cooperative agreement with the National Science Foundation.

This project used data obtained with the Dark Energy Camera (DECam), which was constructed by the Dark Energy Survey (DES) collaboration. Funding for the DES Projects has been provided by the U.S. Department of Energy, the U.S. National Science Foundation, the Ministry of Science and Education of Spain, the Science and Technology Facilities Council of the United Kingdom, the Higher Education Funding Council for England, the National Center for Supercomputing Applications at the University of Illinois at Urbana-Champaign, the Kavli Institute of Cosmological Physics at the University of Chicago, Center for Cosmology and Astro-Particle Physics at the Ohio State University, the Mitchell Institute for Fundamental Physics and Astronomy at Texas A&M University, Financiadora de Estudos e Projetos, Fundacao Carlos Chagas Filho de Amparo, Financiadora de Estudos e Projetos, Fundacao Carlos Chagas Filho de Amparo a Pesquisa do Estado do Rio de Janeiro, Conselho Nacional de Desenvolvimento Cientifico e Tecnologico and the Ministerio da Ciencia, Tecnologia e Inovacao, the Deutsche Forschungsgemeinschaft and the Collaborating

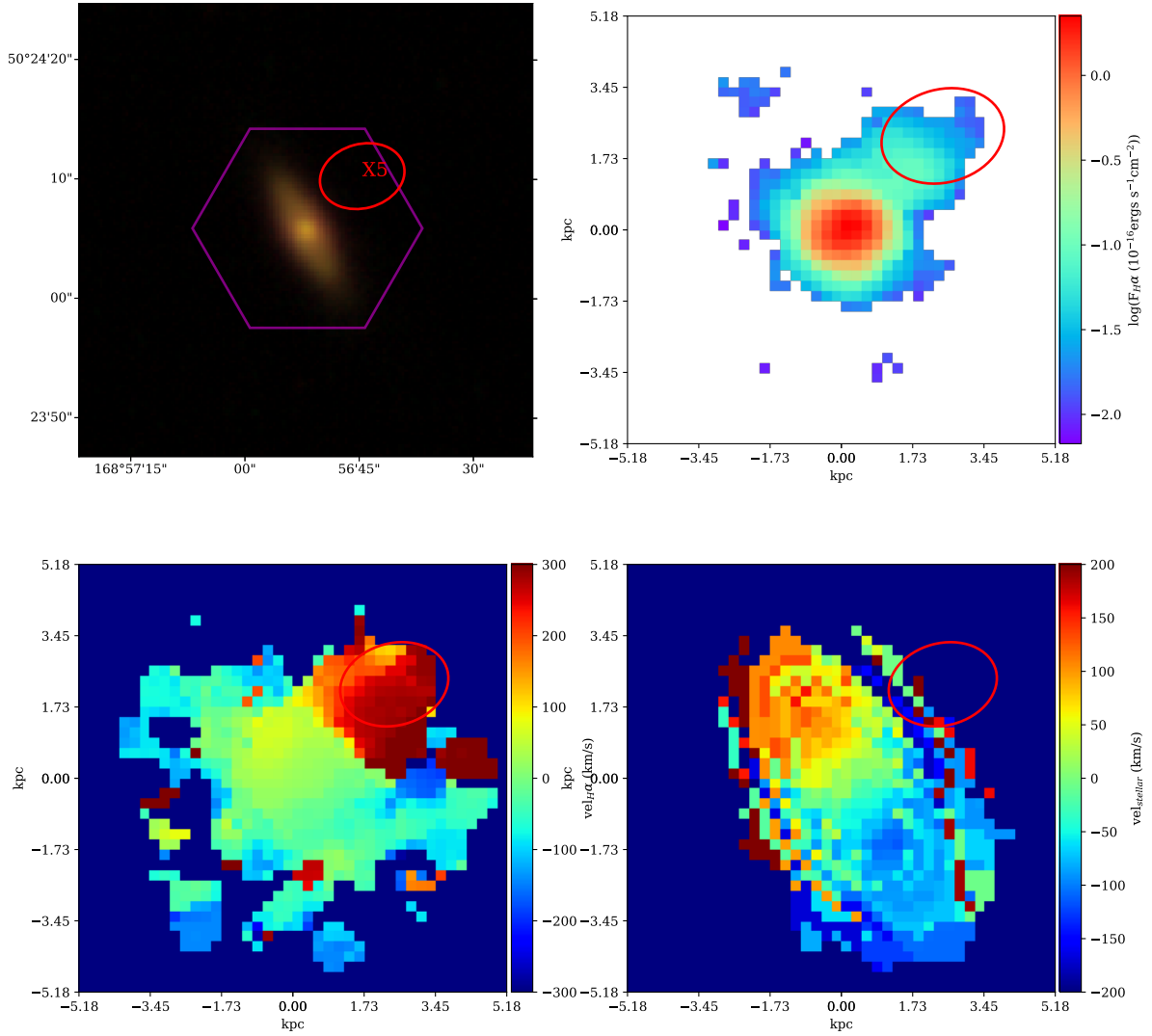


Figure 7. Continued. Here we show the outlying emission for X5.

Institutions in the Dark Energy Survey. The Collaborating Institutions are Argonne National Laboratory, the University of California at Santa Cruz, the University of Cambridge, Centro de Investigaciones Energeticas, Medioambientales y Tecnologicas-Madrid, the University of Chicago, University College London, the DES-Brazil Consortium, the University of Edinburgh, the Eidgenossische Technische Hochschule (ETH) Zurich, Fermi National Accelerator Laboratory, the University of Illinois at Urbana-Champaign, the Institut de Ciències de l'Espai (IEEC/CSIC), the Institut de Física d'Altes Energies, Lawrence Berkeley National Laboratory, the Ludwig-Maximilians Universität München and the associated Excellence Cluster Universe, the University of Michigan, the National Optical Astronomy Observatory, the University of Nottingham, the Ohio State University, the University of Pennsylvania, the University of Portsmouth, SLAC National Accelerator Laboratory, Stanford University, the University of Sussex, and Texas A&M University.

BASS is a key project of the Telescope Access Program (TAP), which has been funded by the National Astronomical Observatories of China, the Chinese Academy of Sciences (the Strategic Priority Research Program "The Emergence

of Cosmological Structures" Grant # XDB09000000), and the Special Fund for Astronomy from the Ministry of Finance. The BASS is also supported by the External Cooperation Program of Chinese Academy of Sciences (Grant # 114A11KYSB20160057), and Chinese National Natural Science Foundation (Grant # 11433005).

The Legacy Survey team makes use of data products from the Near-Earth Object Wide-field Infrared Survey Explorer (NEOWISE), which is a project of the Jet Propulsion Laboratory/California Institute of Technology. NEOWISE is funded by the National Aeronautics and Space Administration.

The Legacy Surveys imaging of the DESI footprint is supported by the Director, Office of Science, Office of High Energy Physics of the U.S. Department of Energy under Contract No. DE-AC02-05CH1123, by the National Energy Research Scientific Computing Center, a DOE Office of Science User Facility under the same contract; and by the U.S. National Science Foundation, Division of Astronomical Sciences under Contract No. AST-0950945 to NOAO.

REFERENCES

- Abolfathi B., et al., 2017, preprint, ([arXiv:1707.09322](#))
- Baldwin J. A., Phillips M. M., Terlevich R., 1981, *PASP*, **93**, 5
- Belfiore F., et al., 2016, *MNRAS*, **461**, 3111
- Bland J., Tully B., 1988, *Nature*, **334**, 43
- Bryant J. J., et al., 2015, *MNRAS*, **447**, 2857
- Bundy K., et al., 2015, *ApJ*, **798**, 7
- Cardelli J. A., Clayton G. C., Mathis J. S., 1989, *ApJ*, **345**, 245
- Cheung E., et al., 2016, *ApJ*, **832**, 182
- Cid Fernandes R., Stasińska G., Schlickmann M. S., Mateus A., Vale Asari N., Schoenell W., Sodré L., 2010, *MNRAS*, **403**, 1036
- Cid Fernandes R., et al., 2013, *A&A*, **557**, A86
- Devine D., Bally J., 1999, *ApJ*, **510**, 197
- Drory N., et al., 2015, *AJ*, **149**, 77
- Epinat B., et al., 2018, *A&A*, **609**, A40
- Farage C. L., McGregor P. J., Dopita M. A., Bicknell G. V., 2010, *ApJ*, **724**, 267
- Fogarty L. M. R., et al., 2012, *ApJ*, **761**, 169
- Graham M. T., et al., 2018, *MNRAS*, **477**, 4711
- Józsa G. I. G., et al., 2009, *A&A*, **500**, L33
- Kauffmann G., et al., 2003, *MNRAS*, **346**, 1055
- Keel W. C., et al., 2012a, *AJ*, **144**, 66
- Keel W. C., et al., 2012b, *MNRAS*, **420**, 878
- Kewley L. J., Groves B., Kauffmann G., Heckman T., 2006, *MNRAS*, **372**, 961
- Law D. R., et al., 2015, *AJ*, **150**, 19
- Law D. R., et al., 2016, *AJ*, **152**, 83
- Lehnert M. D., Heckman T. M., Weaver K. A., 1999, *ApJ*, **523**, 575
- Lin L., et al., 2017, *ApJ*, **837**, 32
- Lintott C. J., et al., 2009, *MNRAS*, **399**, 129
- Lopez Coba C., Sanchez S. F., Bland-Hawthorn J., Moiseev A. V., Cruz-Gonzalez I., Garcia-Benito R., Barrera-Ballesteros J. K., Galbany L., 2018, preprint, ([arXiv:1811.01253](#))
- Lupton R., Blanton M. R., Fekete G., Hogg D. W., O’Mullane W., Szalay A., Wherry N., 2004, *PASP*, **116**, 133
- Maiolino R., et al., 2017, *Nature*, **544**, 202
- Rich J. A., Dopita M. A., Kewley L. J., Rupke D. S. N., 2010, *ApJ*, **721**, 505
- Richards S. N., et al., 2014, *MNRAS*, **445**, 1104
- Sánchez S. F., et al., 2012, *A&A*, **538**, A8
- Sánchez S. F., et al., 2016a, *Rev. Mex. Astron. Astrofis.*, **52**, 21
- Sánchez S. F., et al., 2016b, *Rev. Mex. Astron. Astrofis.*, **52**, 171
- Sánchez S. F., et al., 2018, *Rev. Mex. Astron. Astrofis.*, **54**, 217
- Schawinski K., et al., 2010, *ApJ*, **724**, L30
- Shopbell P. L., Bland-Hawthorn J., 1998, *ApJ*, **493**, 129
- Smee S. A., et al., 2013, *AJ*, **146**, 32
- Tadhunter C., Tsvetanov Z., 1989, *Nature*, **341**, 422
- Unger S. W., Pedlar A., Axon D. J., Whittle M., Meurs E. J. A., Ward M. J., 1987, *MNRAS*, **228**, 671
- Veilleux S., Cecil G., Bland-Hawthorn J., 2005, *ARA&A*, **43**, 769
- Wake D. A., et al., 2017, *AJ*, **154**, 86
- Yan R., et al., 2016, *AJ*, **152**, 197

APPENDIX A: INTEGRATED SPECTRUM OF THE EXTENDED EMITTERS

We used elliptical apertures around the extended emitters to extract the integrated spectrum for each of the sources in our sample, directly from the MaNGA datacube. The integrated spectra are shown in Figure A1-A6. We also show the host galaxy spectrum from the SDSS DR14 spectroscopic survey for reference in the bottom-most panel of each of figure.

APPENDIX B: LIST OF ARTEFACTS FOUND IN THE MANGA DATACUBE

In our visual search for outlying $H\alpha$ emitters in the entire data release 14 of the Sloan Digital Sky Survey (SDSS) IV MaNGA data release, we have found the following list of objects which are found to be artefacts. These artefacts are of two kinds: ones that appear like unresolved blobs (see Table B1) and ones that appear like extended sources. All the unresolved blobs appear like high signal-noise ratio emitters, with a different velocity component (see Fig. 2 in the main text). However, a manual inspection of their spectra shows that their $H\alpha$ FWHM is much narrower than the instrumental width. Additionally, they do not show line emission in other lines like $H\beta$, [OIII], [NII] which usually accompany strong $H\alpha$ emission. We believe that these artefacts are caused by some spurious low-intensity cosmic rays which are not correctly flagged by the MaNGA data reduction pipeline⁴.

The extended emitters shows two types of artefacts, the first type is same as that of the unresolved blobs, which show a very narrow line width, the second kind show a strong $H\alpha$ emission in the PIPE3D output, however there is no emission line in the MaNGA datacube. Moreover, the integrated $H\alpha/H\beta$ emission line ratio is unrealistically higher than expected by any realistic assumptions about the nebular regions. We surmise that such artefacts could be due to incorrect fitting in the PIPE3D pipeline. See Table B2 for the full list.

⁴ <https://www.sdss.org/dr14/manga/manga-caveats/>

Table B1. List of artefacts in the MaNGA datacube which appear like unresolved blobs.

Obj ID	RA J2000 (hhmmss)	DEC J2000 (ddmmss)	plate-ifu	Host SDSS Obj ID	RA (Host) J2000 (deg)	DEC (Host) J2000 (deg)	z
B1	15:28:03.533	+42:48:41.535	7443-9102	1237662501076336774	15:28:03.32	+42:48:49.11	0.0918
B2	03:12:46.534	-01:01:16.964	8081-12701	1237666299480899906	03:12:47.18	-01:01:22.27	0.0818
B3	03:44:31.591	+00:00:14.240	8086-12704	1237663238741622872	03:44:31.59	+00:00:23.94	0.1087
B4	07:30:40.578	+40:11:37.756	8131-6103	1237663530789503529	07:30:40.96	+40:11:30.39	0.1204
B5	08:00:28.325	+41:39:46.527	8143-6103	1237673705042935885	08:00:27.99	+41:39:38.32	0.0438
B6	07:51:14.337	+28:09:05.193	8146-9102	1237657630579163404	07:51:14.77	+28:09:13.01	0.0526
B7	07:58:25.691	+27:09:44.698	8149-12702	1237657773924417752	07:58:26.21	+27:09:41.50	0.0473
B8	07:49:38.378	+48:30:53.394	8239-9102	1237663786879942876	07:49:37.25	+48:30:56.46	0.0229
B9	09:07:18.893	+41:23:18.897	8247-6102	1237657775543746865	09:07:18.10	+41:23:18.33	0.0273
B10	11:08:01.255	+46:51:09.80	8257-12703	1237660636535652531	11:08:00.70	+46:51:03.66	0.0252
B11	12:00:42.109	+43:21:14.227	8259-12705	1237661968502358077	12:00:41.45	+43:21:16.47	0.1131
B12	12:17:32.214	+43:45:25.412	8262-3704	1237661871329640526	12:17:32.74	+43:45:26.50	0.0244
B13	14:20:04.917	+47:07:08.663	8326-6102	1237661957225119836	14:20:04.29	+47:07:16.82	0.07038
B14	13:58:33.421	+41:43:32.770	8332-3704	1237661850403602575	13:58:33.54	+41:43:27.00	0.0431
B15	11:31:20.193	+21:25:41.810	8338-12705	1237667734503882923	11:31:20.04	+21:25:28.85	0.1337
B16	13:46:48.895	+39:04:48.592	8447-12702	1237664296371421207	13:46:49.38	+39:05:01.32	0.0618
B17	09:49:31.512	+42:07:34.148	8459-12701	1237660637066100922	09:49:30.96	+42:07:48.99	0.0721
B18	15:55:47.193	+56:07:37.761	8481-3703	1237651539797737641	15:55:46.82	+56:07:31.92	0.0423
B19	16:00:44.508	+53:46:24.932	8481-3704	1237651538724978813	16:00:44.81	+53:46:31.93	0.1104
B20	16:27:45.899	+44:10:29.753	8484-9101	1237655128765235356	16:27:46.29	+44:10:39.00	0.1398
B21	15:31:17.835	+45:25:11.211	8551-12702	1237661386000826593	15:31:17.56	+45:24:59.53	0.07051
B22	07:39:07.686	+41:23:33.537	8566-6102	1237673310428856407	07:39:07.71	+41:23:39.42	0.0986
B23	10:22:09.520	+38:31:01.478	8568-12704	1237661137960632446	10:22:10.31	+38:31:04.17	0.0533
B24	16:32:32.982	+39:07:39.957	8603-12701	1237659326566564084	16:32:33.73	+39:07:51.74	0.1306
B25	21:10:15.857	+10:24:20.440	8618-12705	1237653008120610948	21:10:16.51	+10:24:31.63	0.1186
B26	08:10:42.094	+48:55:06.267	8720-6104	1237651496296382666	08:10:42.56	+48:55:07.58	0.03864
B27	08:52:41.457	+54:25:57.881	8724-9101	1237651192432885982	08:52:40.82	+54:26:03.09	0.0386
B28	10:25:42.860	+36:01:31.483	8943-12704	1237662224594436134	10:25:43.87	+36:01:24.98	0.0546
B29	14:48:51.586	+30:33:43.129	9002-12701	1237662696493547575	14:48:50.84	+30:33:51.74	0.061

Notes. Column (1) gives the object ID of the outlying H α emitter, column (2) and (3) gives the RA and DEC of the outlying H α emitter respectively. Columns (4) and (5) give the MaNGA plateifu name and SDSS DR14 object ID of the host galaxy respectively. And columns (6), (7) and (8) give the RA and DEC and SDSS spectroscopic redshift of the host galaxy respectively.

Table B2. List of artefacts in the MaNGA datacube with extended features.

Obj ID	RA J2000 (hhmmss)	DEC J2000 (ddmmss)	plate-ifu	Host SDSS Obj ID	RA (Host) J2000 (deg)	DEC (Host) J2000 (deg)	z
X6 ^a	08:20:52.800	+18:01:04.896	8241-12702	1237667142860407201	08:20:52.48	+18:00:55.96	0.0441
X7 ^b	10:28:15.339	+42:58:07.480	8253-12701	1237660634384761005	10:28:14.10	+42:58:05.32	0.0452
X8 ^a	23:50:35.753	-1:07:52.374	8655-12705	1237663275779227768	23:50:36.42	-01:07:40.97	0.0456
X9 ^a	07:46:03.970	+39:53:23.003	8713-12702	1237651192424890568	07:46:04.58	+39:53:11.06	0.0418
X10 ^b	12:59:12.968	+27:46:32.067	8931-6103	1237667323797700611	12:59:13.49	+27:46:28.53	0.0231
X11 ^a	15:29:43.233	+27:06:47.309	9042-12701	1237662697034613032	15:29:44.01	+27:06:43.18	0.0457

Notes. Column (1) gives the object ID of the outlying H α emitter where X#^a represents artefact due to the PIPE3D pipeline and X#^b represents artefact due to a spurious cosmic ray, column (2) and (3) gives the RA and DEC of the outlying H α emitter respectively. Column (4) and (5) gives the MaNGA plateifu name and SDSS DR14 object ID of the host galaxy respectively. And column (6), (7) and (8) gives the RA and DEC and SDSS spectroscopic redshift of the host galaxy respectively.

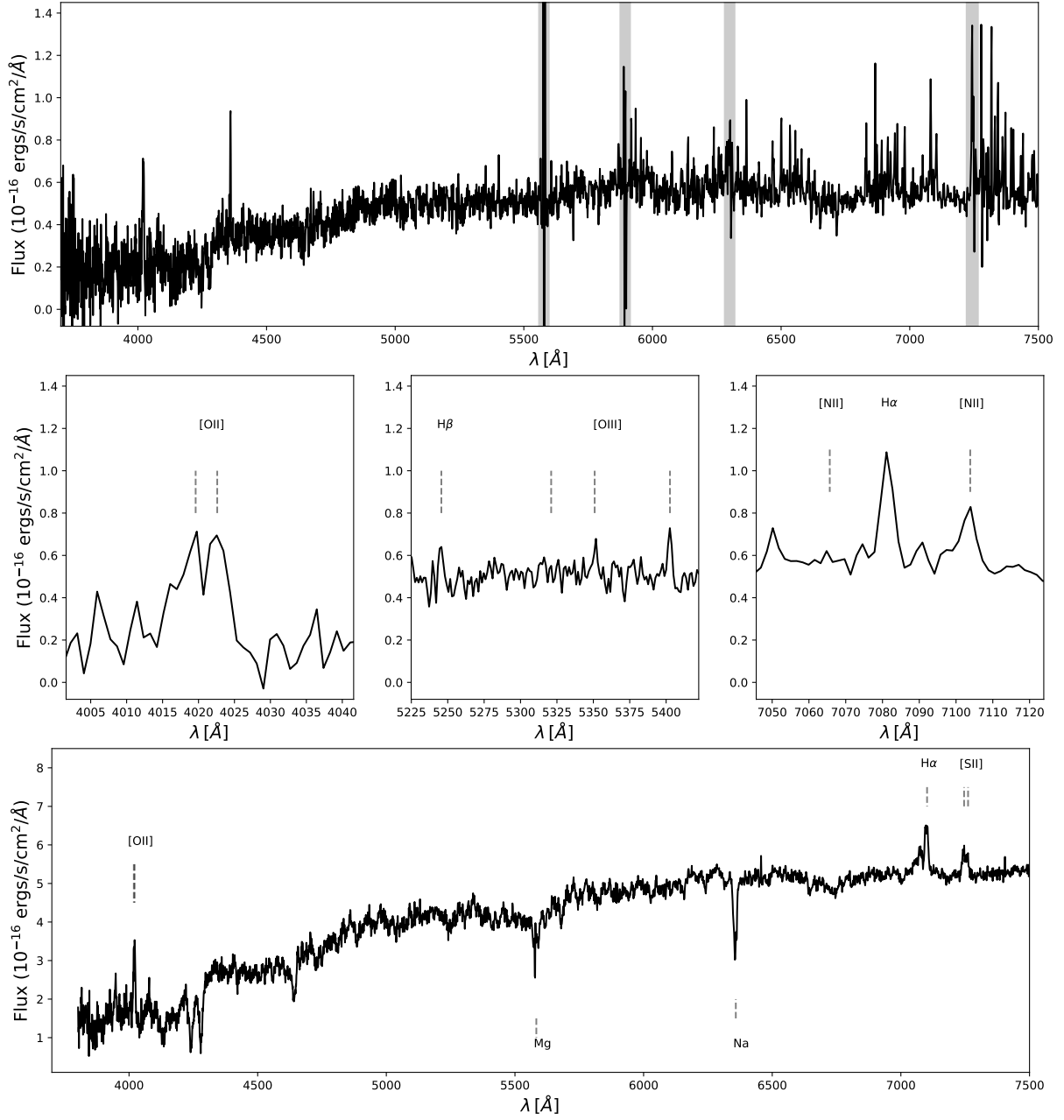


Figure A1. Top: Integrated spectrum for X1. The grey shaded regions indicate regions with strong sky lines in the SDSS spectrum. Middle: A zoomed-in spectrum around the [OII] doublet (left), [OIII] λ 4960, 4963, and 5007 and H β (middle), and H α and the [NII] doublet (right). Bottom: Observed frame host galaxy spectrum from the SDSS DR14 spectroscopic survey.

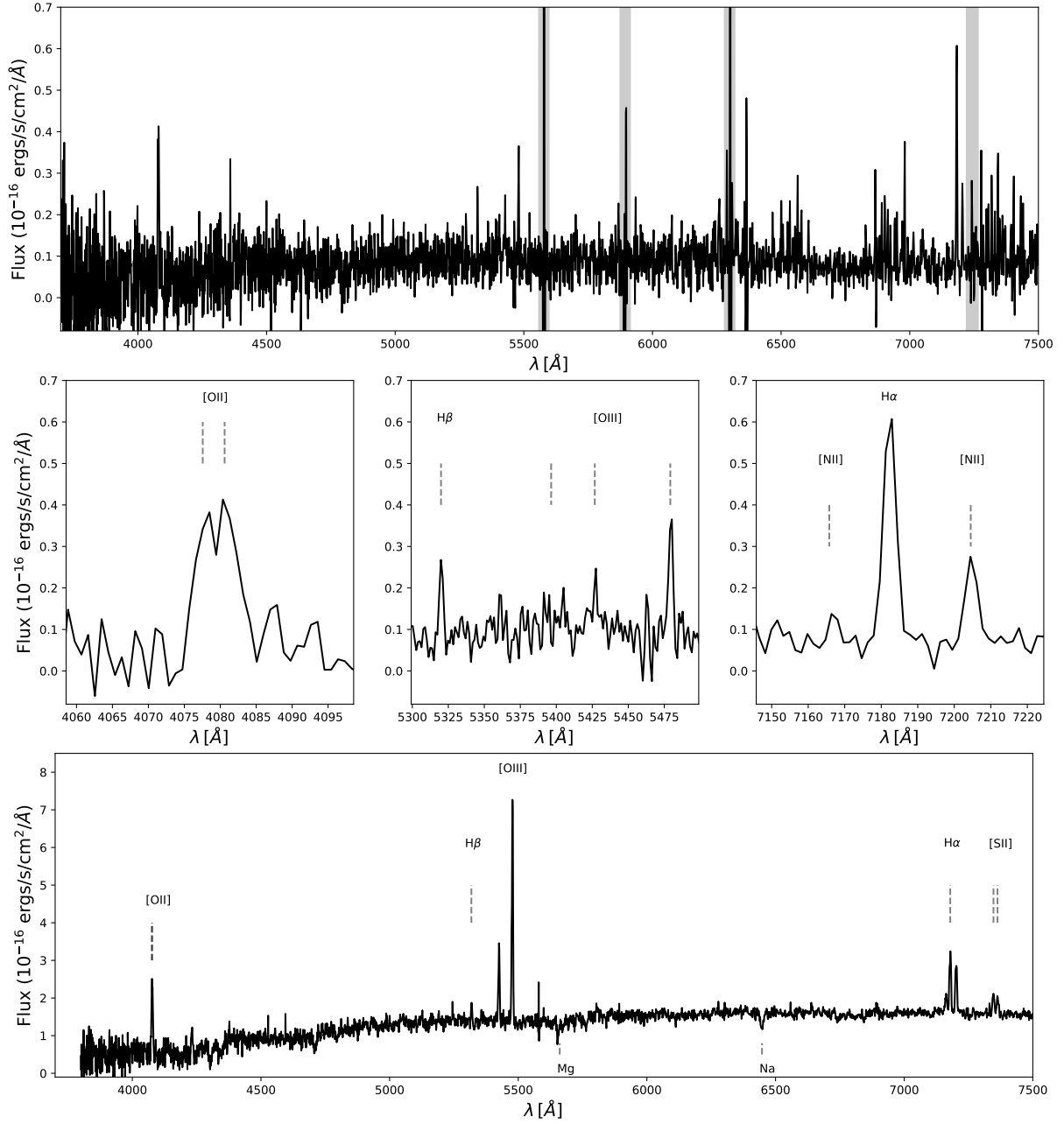


Figure A2. Continued. Here we show the integrated spectrum for X2.1 and its corresponding host galaxy.

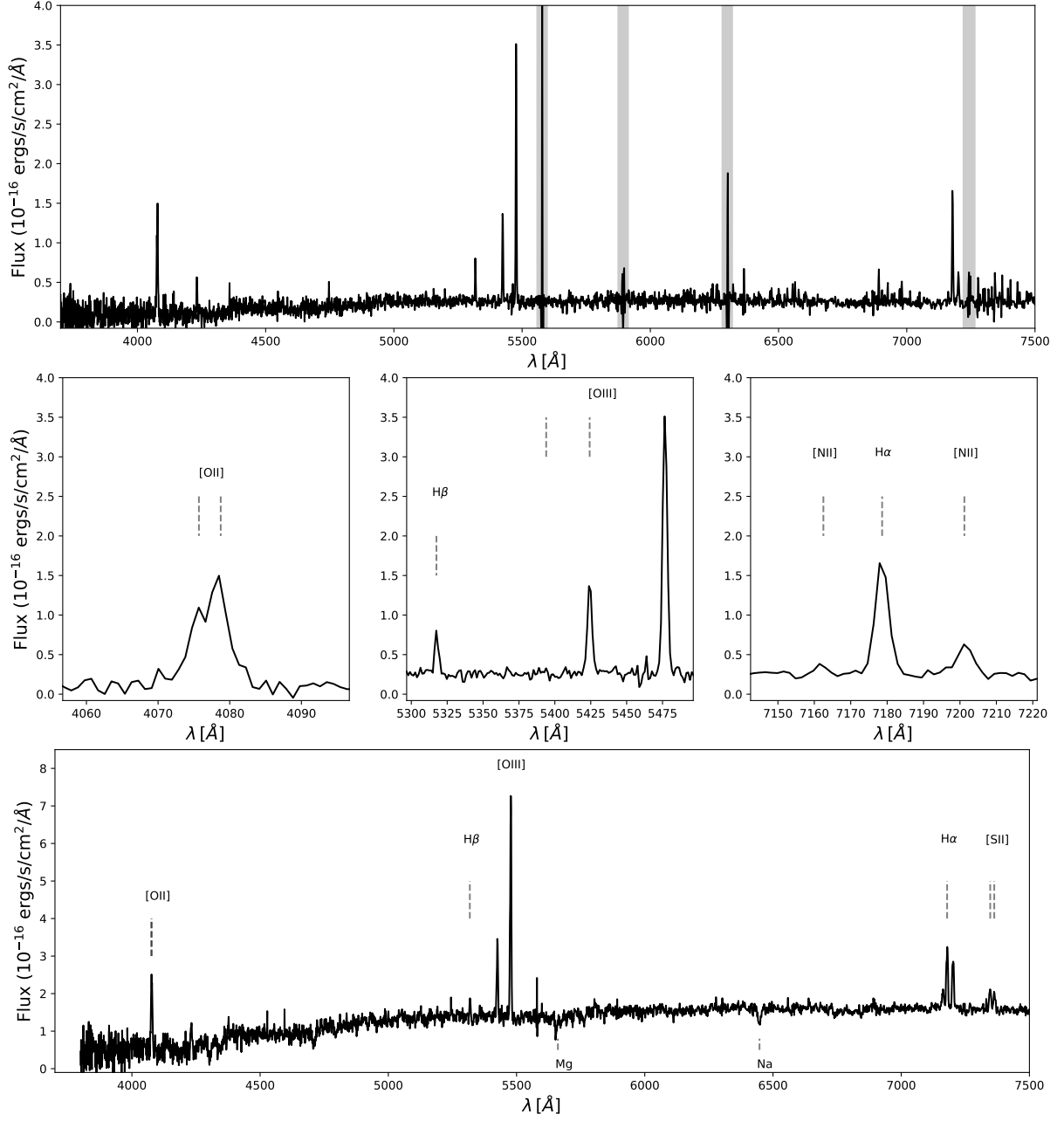


Figure A3. Continued. Here we show the integrated spectrum for X2.2 and its corresponding host galaxy.

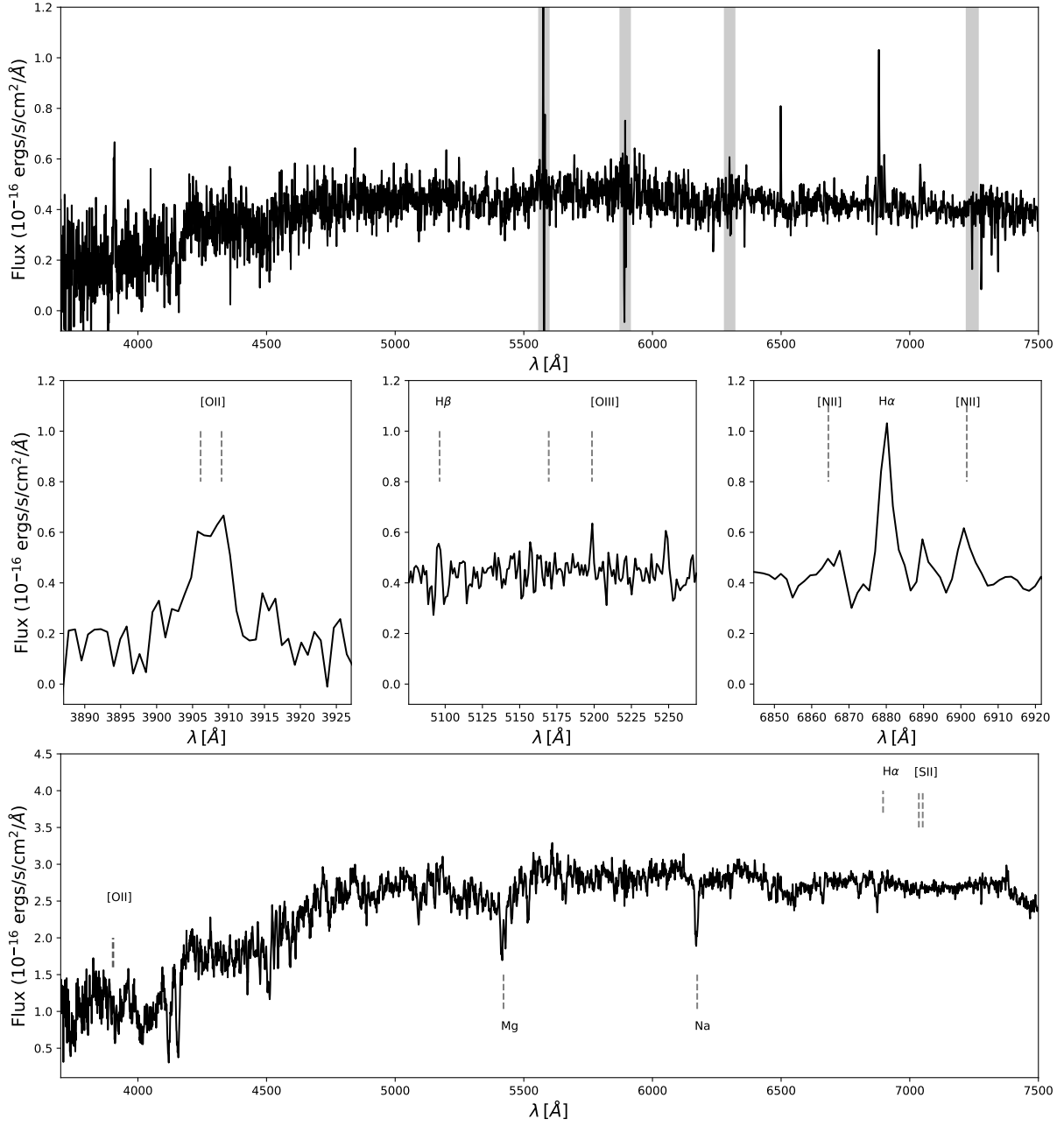


Figure A4. Continued. Here we show the integrated spectrum for X3 and its corresponding host galaxy.

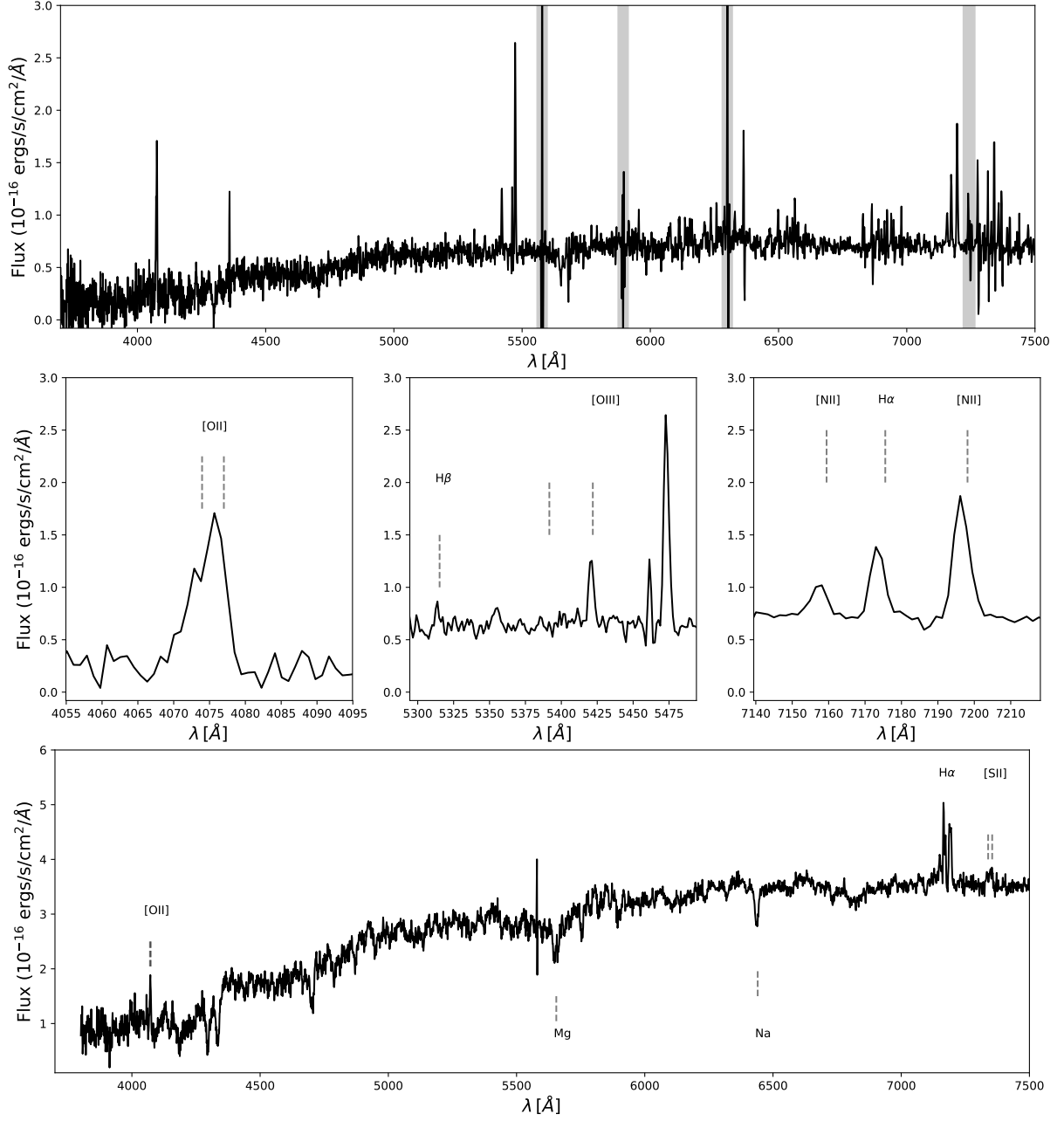


Figure A5. Continued. Here we show the integrated spectrum for X4 and its corresponding host galaxy.

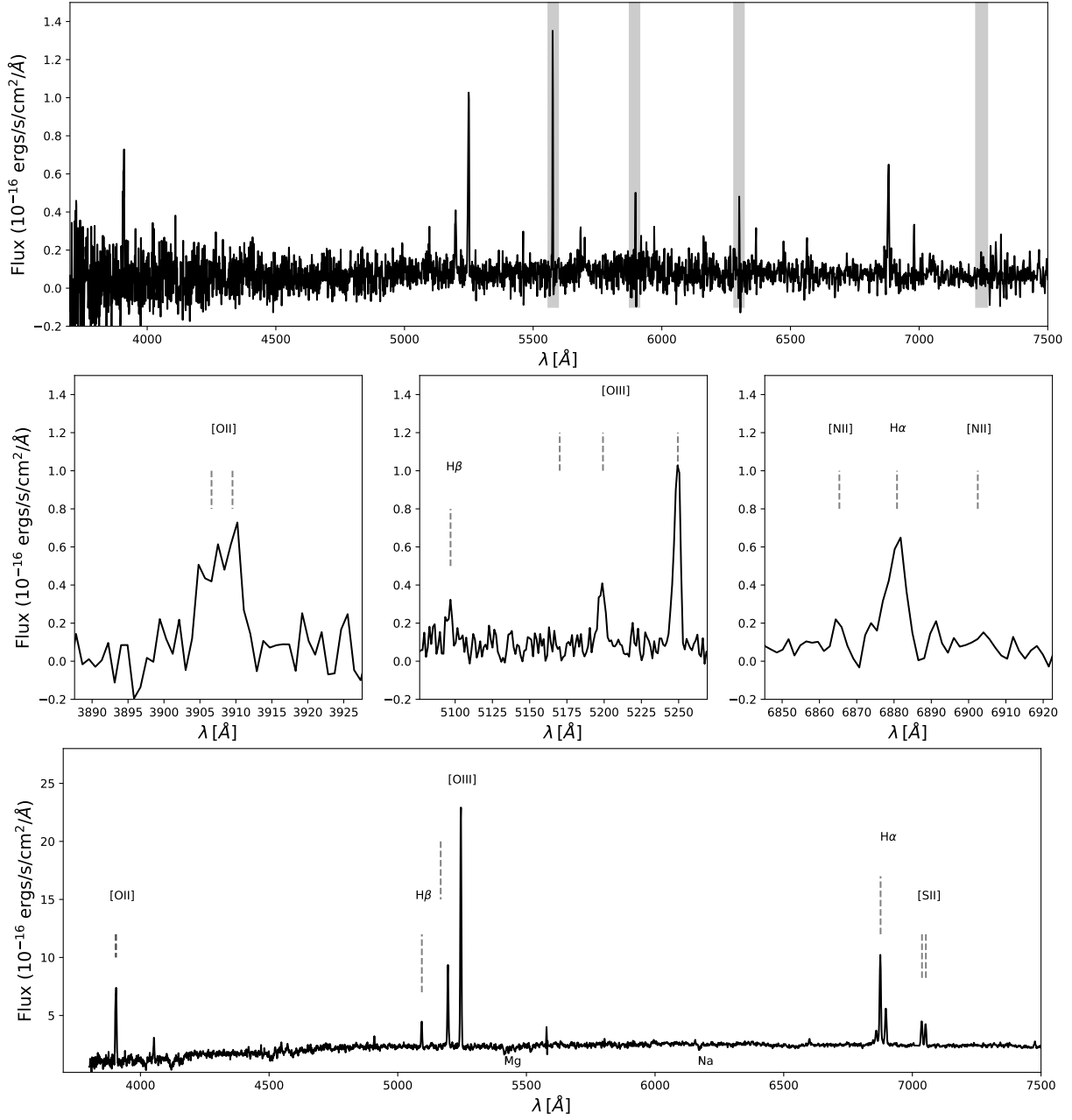


Figure A6. Continued. Here we show the integrated spectrum for X5 and its corresponding host galaxy.